

ISSN: 0256-307X

中国物理快报

Chinese Physics Letters

Volume 29 Number 11 November 2012

A Series Journal of the Chinese Physical Society
Distributed by IOP Publishing

Online: <http://iopscience.iop.org/cpl>
<http://cpl.iphy.ac.cn>

CHINESE PHYSICAL SOCIETY
IOP Publishing

JUST FOR AUTHORS
— CHINESE PHYSICS LETTERS

Preparation and Characterization of Fe-Based Metallic Glasses with Pure and Raw Elements *

Nassima Seghairi^{1,2}, Badis Bendjemil^{1,3,4**}, Gabriel Lavorato¹, Alberto Castellero¹, Marcello Baricco¹

¹Dipartimento di Chimica I.F.M./NIS/CNISM/INSTM, Università di Torino, Via Giuria 9, 10125 Trino, Italy

²University of Larbi Ben M'hidi, Oum El Bouaghi, Algeria

³LASEA, Faculty of Sciences, Department of Chemistry, University of Annaba, Algeria

⁴University of Guelma, P. O. Box 12, 24000 Guelma, Algeria

(Received 10 July 2012)

Amorphous alloys with a composition (at.%) $\text{Fe}_{48}\text{Cr}_{15}\text{Mo}_{14}\text{C}_{15}\text{B}_6\text{Y}_2$ were prepared by using either pure elements (alloy B1) or a commercial AISI430 steel as a base material (B2). When prepared from pure elements, alloy (B1) could be cast in plate form with a fixed thickness of 2 mm and variable lengths between 10 and 20 mm by means of copper-mold injection in an air atmosphere. In the case of alloy B2, prepared by using commercial grade raw materials, rods of 2 mm diameter are obtained. Ribbons (B1 and B2) of width 5 mm and thickness about 30 μm are prepared from the arc-melted ingots using a single roller melt spinner at a wheel speed of 40 m/s. The thermal and structural properties of the samples are measured by a combination of differential scanning calorimetry (DSC), x-ray diffraction and scanning electron microscopy. Chemical compositions are checked by energy dispersive spectroscopy analysis. X-ray diffraction and scanning electron microscopy observations confirm that an amorphous structure is obtained in all the samples. A minor fraction of crystalline phases (oxides and carbides) is detected on the as-cast surface. Values of hardness and Young modulus were measured by nanoindentation for both the alloys. The effects of adverse casting conditions (such as air atmosphere, non-conventional injection copper mold casting and the partial replacement of pure elements with commercial grade raw materials) on the glass formation and properties of the alloy are discussed.

PACS: 81.05.Kf, 73.50.-h, 07.85.Fv, 07.20.Fw

DOI: 10.1088/0256-307X/29/11/118102

Since the first Fe-based metallic glasses of the Fe-P-C alloy were synthesized in 1967,^[1] Fe-based metallic glasses, which have good soft magnetic properties, excellent mechanical properties and corrosion resistance, have attracted much attention from researchers interested in amorphous alloys. Recently, Fe-based bulk metallic glasses (BMGs) were obtained in many systems.

However, high cooling rates are essential during preparation to avoid crystallization. This condition limits further applications of Fe-based metallic glasses because of the limitation of sample size in two or one dimensions, i.e., only sheets or wires can be produced.^[2] Recently, Fe-based bulk metallic glasses (BMGs) were obtained in many systems. Inoue and Al succeeded in fabricating Fe-based bulk metallic glasses from high purity raw materials by copper mould casting in the following systems: Fe-(Al,Ga)-P-C-B,^[3] Fe-(Zr,Hf,Nb,Ta)-B,^[4] Fe-Co-Ln-B,^[5] and Fe-(Cr,Moand/orNb)-B-C.^[6] Improvement of the soft magnetic properties in Fe-based bulk metallic glass is reported by adding a small amount of Ni.^[7] However, during the last decade, these materials could be prepared with a lower Fe content showing a paramagnetic behavior at room temperature. These materials were named structural amorphous steels (SAS)^[8,9]

and today can be produced with a maximum thickness of 16 mm.^[10] In this Letter, we study the effect of some processing conditions (air atmosphere, casting of a plate and use of commercial raw materials) on the glass formation and properties of Fe-based BMGs.

Samples with the composition $\text{Fe}_{48}\text{Cr}_{15}\text{Mo}_{14}\text{C}_{15}\text{B}_6\text{Y}_2$ (alloy B1) were fabricated using pure elements. In order to evaluate the possibility of an industrial scale production of the structural amorphous steels, a yttrium containing system (alloy B2) was also prepared using an AISI430 steel (55.7wt%) and a commercial grade FeB alloy (7.3wt%) as base materials; the desired stoichiometry was obtained by adding Mo (25.7wt%), C (3.4wt%), Cr (5.4wt%) and Y (3.4wt%) in the form of pure elements. Master alloys were produced by arc-melting under an Ar atmosphere. The samples were re-melted in an induction furnace and quenched in air atmosphere into a water-cooled copper mould in order to obtain a glassy structure. A B1 plate was produced using a mould with a rectangular cavity of width 20 mm and a fixed thickness of 2 mm. A B2 alloy was cast in a rod shape using a cylindrical copper mould of 2 mm in diameter. Ribbons (B1 and B2) of width 5 mm and thickness about 30 μm were prepared from the arc-melted ingots using a single roller melt spinner at a wheel speed of

*Supported by Regione Piemonte under Grant No D23, and the WWS Project of the University of Torino.

**Corresponding author. Email: badis23@ymail.com

© 2012 Chinese Physical Society and IOP Publishing Ltd

40 m/s. The amorphous character was identified by x-ray diffraction (XRD) using the Philips PW1830 (Co K α , $\lambda = 1.7897 \text{ \AA}$) diffractometer. All the XRD patterns will be reported as a function of the wave vector $S = 4\pi\sin(\theta)/\lambda$, where θ corresponds to the scattering angle. Scanning electron microscopy (SEM) investigations were performed using a Leica Stereoscan 420 microscope instrument, and chemical compositions were checked by energy dispersive spectroscopy (EDS) analysis. Thermal analysis was performed in a Perkin Elmer Diamond differential scanning calorimeter (DSC) and in a Setaram high-temperature differential scanning calorimeter (HTDSC) at a heating rate of 0.17 K/s. Nanoindentation tests were carried out with a Fischerscope HM2000 employing a Vickers indenter. Several indents were performed to make sure that the maximum penetration displacement was significantly lower than 1/10 of the sample thickness. Values of indentation hardness H_{IT} and elastic indentation modulus E_{IT} were obtained from the loading and unloading curves, respectively, according to the procedure proposed by Oliver and Pharr.^[11]

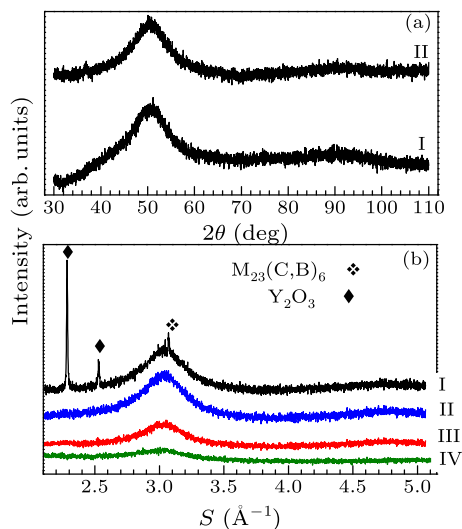


Fig. 1. (a) XRD patterns: ribbon of alloy B1 (I), ribbon of alloy B2 (II). (b) XRD patterns of the bulk: B1 as cast surface (I), B1 polished surface (II), B1 cross-section (III), B2 cross-section (IV).

The XRD patterns of samples B1 (curve I in Fig. 1(a)) and B2 (curve II in Fig. 1(a)) ribbons show an amorphous halo without evidence of crystalline peaks, suggesting fully amorphous structures. The diffraction patterns of samples alloy B1 and B2 bulk are shown in Fig. 1(b). In the case of samples B1, the XRD patterns of the as-cast surface of the plates (curve I in Fig. 1(b)) show the typical halo of the amorphous structure, together with some diffraction peaks corresponding to $M_{23}(B,C)_6$ and Y_2O_3 phases. Similar observations have already been reported in similar Fe-based BMGs.^[12] After removing a layer of about 0.1 mm from the outer surface, no crystalline diffrac-

tion peaks can be detected on the polished surface of sample B1 (curve II in Fig. 1(b)), indicating that the crystalline phases previously observed is mainly located on the surface. The formation of the crystalline phases at the surface can likely be attributed to the presence of oxygen contaminations in the casting atmosphere and to the presence of imperfections on the mould surface.^[13]

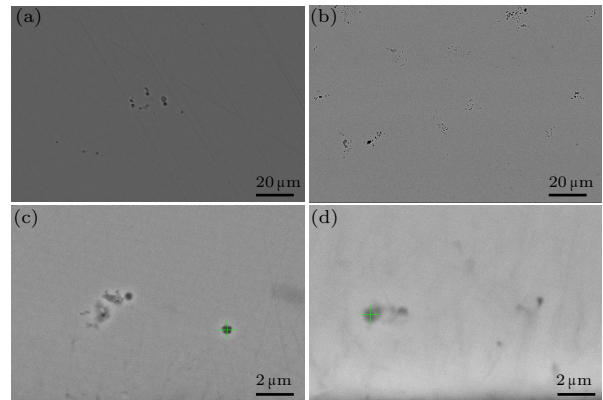


Fig. 2. SEM backscattered electron images for (a) as-cast of alloy B2 BMG, (b) as-cast of alloy B1 BMG, (c) as-cast ribbons of alloy B2, and (d) as-cast ribbons of alloy B1.

The XRD patterns of the cross-section of sample B1 (curve III in Fig. 1(b)) present a broad diffraction halo that is consistent with the presence of an amorphous structure. Nevertheless, the presence of a small fraction of crystalline phases, mainly at the surface, which could not be detected by XRD, cannot be ruled out. In the case of the cross section of the rod of sample B2, the XRD pattern does not present any crystalline diffraction peak (curve IV in Fig. 1(b)), indicating the presence an amorphous structure.

The back scattered SEM images of the as-cast samples are shown in Fig. 2. Chemical analysis was obtained by EDS only for metals, because light elements cannot be detected with accuracy. The SEM back scattering micrograph of the cross-section taken from the top-middle part of sample B2 is shown in Fig. 2(a). It is possible to distinguish some micrometric sized precipitates that are homogeneously distributed across the section. EDS chemical analysis reveals that the precipitates present a very high fraction of Y and O, while the surrounding amorphous matrix has less Y content than expected. The same phenomenon is found for B1 alloy BMG (Fig. 2(b)), B2 alloy ribbon (Fig. 2(c)), and B1 alloy ribbon (Fig. 2(d)). The SEM results are in agreement with the detection of yttrium oxide from XRD patterns and confirm that they are formed not only on the surface but also inside the plate and ribbon. Additionally, Y_2O_3 is found, which is certainly formed due to the high reactivity of yttrium with the rest of the oxygen in the argon atmosphere. It is known that minor addition of rare earth elements (REs) is a powerful mean for modifying

the properties and the glass forming ability of metallic glasses, and it has already been employed in Fe-based BMGs.^[14] The oxygen scavenging effects of REs is to retard the nucleation and growth of carbides, stabilizing the undercooled melt and, consequently, favoring the amorphization.^[8]

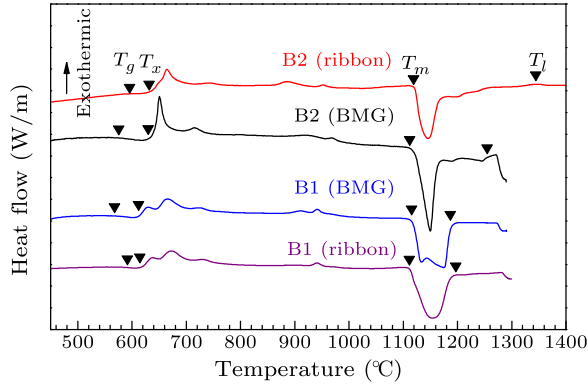


Fig. 3. HTDSC curves of as-cast bulk and ribbons.

The crystallization and melting curves behavior of the amorphous sample from all the alloys has been studied by high temperature differential scanning calorimeter (HTDSC) at a heating rate of 10 K/min and the results are shown in Fig. 3. In order to identify the glass transition temperature T_g and crystallization temperature T_x , the experiment was repeated with the conventional DSC, for the same as-cast sample, as shown in Fig. 4. The main characteristic temperatures and the thermal parameters describing the glass forming ability are listed in Table 1. The thermograms of sample B1 (BMG) reveal a non-eutectic melting, whereas B1(ribbon), B2(BMG) and B2(ribbon) melts in a single endothermic peak. In the case

of the B2 samples, the melting temperature appears in high temperature events that might be due to the melting of impurities present in the commercial grade raw materials. The apparent liquidus temperature of the B2 samples is significantly higher than the one observed for the B1 samples leading to a decrease of the parameter used for assessing the glass forming ability. The maximum amorphous thickness achievable (critical casting thickness) is at least 2 mm in the case of the B2 (BMG) alloy. However, it is expected that the use of raw materials tends to reduce it with respect to the use of pure elements. The reduction on the GFA can be inferred from differences in γ parameter (0.349 for B1 and 0.344 for B2) which has been suggested to be correlated with the critical thickness.^[15] In the case of the B1 samples, the HTDSC traces of crystallization appear to be very similar for ribbons and BMG.

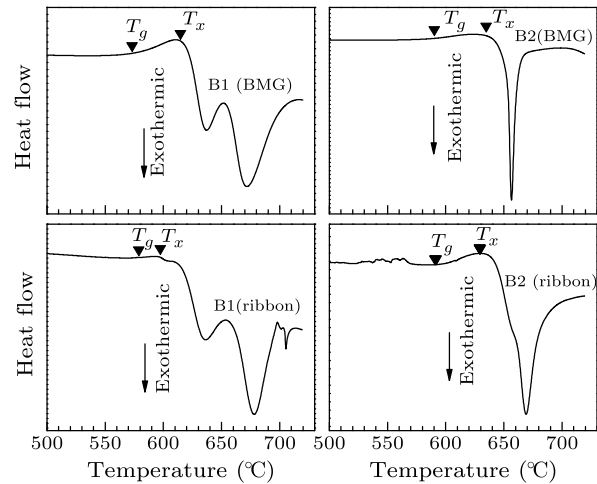


Fig. 4. DSC curves of as-cast bulk and ribbons.

Table 1. Thermal and mechanical properties of samples B1 and B2.

	T_g (°C)	T_x (°C)	T_m (°C)	T_l (°C)	γ	H (GPa)	E (GPa)
B1 BMG	573	615	1116	1187	0.349	13.1 ± 0.4	174 ± 23
B2 BMG	590	635	1122	1255	0.344	16.73 ± 3.83	192.49 ± 3.3
B1 ribbon	579	597	1100	1197	0.336	14.89 ± 2.36	153.99 ± 1.33
B2 ribbon	595	632	1114	1344	0.325	16.29 ± 2.7	166.34 ± 1.69

DSC curves of the four samples of alloys exhibit the sequential transition of amorphous solid, glass transition, supercooled liquid and then crystallization, as shown in Fig. 4. The DSC scan of sample B2 (BMG) exhibits the characteristic wide supercooled liquid region. The sample crystallises through a sharp single exothermic crystallization peak. Pursuant to DSC scans for the samples B1 bulk and ribbon, the crystallization gives various overlapped exothermic peaks. The crystallization products likely constitute a metastable mixture, as evidenced by the small exothermic peak at about 940°C.^[9]

Nanoindentation tests were performed on the polished surfaces of samples B1 (BMG and ribbon) and B2 (BMG and ribbon). The hardness and elastic modulus were found to be 13.1 ± 0.4 GPa and 174 ± 23 GPa, respectively, for alloy B1(BMG) and 16.73 ± 3.83 GPa and 192.49 ± 3.3 GPa, respectively, for alloy B2 (BMG) and 14.89 ± 2.36 GPa and 153.99 ± 1.33 GPa, respectively, for alloy B1(ribbon) and 16.29 ± 2.7 GPa and 166.34 ± 1.69 GPa, respectively, for alloy B2(ribbon), as listed in Table 1. Such values are in agreement with the results previously reported for the same alloy prepared with pure elements and conventional injection casting technique ($H = 13$ GPa, $E = 180$ – 200 GPa)^[9] as well as for alloys with similar compo-

isied surfaces of samples B1 (BMG and ribbon) and B2 (BMG and ribbon). The hardness and elastic modulus were found to be 13.1 ± 0.4 GPa and 174 ± 23 GPa, respectively, for alloy B1(BMG) and 16.73 ± 3.83 GPa and 192.49 ± 3.3 GPa, respectively, for alloy B2 (BMG) and 14.89 ± 2.36 GPa and 153.99 ± 1.33 GPa, respectively, for alloy B1(ribbon) and 16.29 ± 2.7 GPa and 166.34 ± 1.69 GPa, respectively, for alloy B2(ribbon), as listed in Table 1. Such values are in agreement with the results previously reported for the same alloy prepared with pure elements and conventional injection casting technique ($H = 13$ GPa, $E = 180$ – 200 GPa)^[9] as well as for alloys with similar compo-

sition ($H = 13.8$ GPa).^[8] In addition, nanoindentation hardness values do not show significant variation across the sample B2, suggesting that there are not local changes of composition and microstructure.

Three different Fe-Cr-Mo-C-based structural amorphous steels have been successfully prepared with the purpose of testing the possible industrial development of these kind of alloys: (i) they are all prepared in air atmosphere, (ii) as an approach to near-net-shape fabrication, two of them are obtained in a rectangular 2-mm-thick plate shape, and (iii) AISI 430 commercial steel is employed as the raw material in the synthesis of the third alloy. The amorphous formation during quenching from the liquid state was promoted by minor alloying of Y, confirming previous studies. Minor alloying with REs is exploited to successfully obtain 2-mm-thick amorphous plates, suggesting that the formation crystalline phases can be avoided when the oxygen is removed from the melt by forming innocuous oxides. This seems to be a promising approach for the synthesis of BMGs and ribbons starting from commercial grade raw materials in view of an industrial production. No major difference in the structural or thermal properties of both alloys is detected, but the thermal stability of the alloy made from commercial steel is significantly reduced. The structural and mechanical characterization are in agreement with the values previously reported in the literature. The results obtained in this work represent a promising step in view of the industrial application

of this type of materials that are likely to be employed in the future as biomedical instruments, die tools, sport goods and specific functional materials.

The authors are grateful to INRIM, Torino for providing experimental facilities.

References

- [1] Duwez P and Lin S C H 1967 *J. Appl. Phys.* **38** 4096
- [2] Haigiwara M, Inoue A and Masumoto T 1982 *Metall. Trans.* **13A** 373
- [3] Inoue A, Shinohara Y and Gook J S 1995 *Mater. Trans. JIM* **36** 1427
- [4] Inoue A, Zhang T, Itoi T and Takeuchi A 1997 *Mater. Trans. JIM* **38** 359
- [5] Zhang W and Inoue A 2000 *Mater. Trans. JIM* **41** 1679
- [6] Pang S, Zhang T, Asami K and Inoue A 2001 *Mater. Trans. JIM* **42** 376
- [7] Wang W H, Pan M X, Zhao D Q, Hu Y and Y Bai H J 2004 *J. Phys.: Condens. Matter* **16** 3719
- [8] Lu Z P, Liu C T, Thompson J R and Porter W D 2004 *Phys. Rev. Lett.* **92** 245503
- [9] Ponnambalam V, Poon S J and Shiflet G J 2004 *J. Mater. Res.* **19** 1320
- [10] Shen J, Chen Q, Sun J, Fan H and Wang G 2005 *Appl. Phys. Lett.* **86** 151907
- [11] Oliver W C and Pharr G M 1992 *J. Mater. Res.* **7** 1564
- [12] Pan J, Chen Q, Li N and Liu L 2008 *J. Alloys Compd.* **463** 246
- [13] Kramer M J, Mecco H, Dennis K W, Vargonova E, McCallum R W and Napolitano R E 2007 *J. Non-Cryst. Solids* **353** 3633
- [14] Wang W H 2007 *Prog. Mater. Sci.* **52** 540
- [15] Lu Z P and Liu C T 2002 *Acta Mater.* **50** 3501

Chinese Physics Letters

Volume 29

Number 11

November 2012

GENERAL

- 110201 **Solution of Multimaterial Equilibrium Radiation Diffusion Problems by using the Discontinuous Galerkin Method**
ZHANG Rong-Pei, YU Xi-Jun, ZHU Jiang
- 110301 **Quantum Information Theoretical Analysis of Quantum Secret Sharing**
XIAO He-Ling, GUO Wang-Mei, WANG Xiao
- 110302 **Analytical Solutions to the Time-Independent Gross-Pitaevskii Equation with a Harmonic Trap**
SHI Yu-Ren, WANG Guang-Hui, LIU Cong-Bo, ZHOU Zhi-Gang, YANG Hong-Juan
- 110303 **Laser-Catalyzed Domain Formation in Spinor-1 Bose Condensates**
JIANG Ya-Jing, SUN Jing-Xin, JING Hui
- 110304 **Pseudo-Harmonic Oscillatory Ring-Shaped Potential in a Relativistic Equation**
M. Eshghi
- 110305 **Cryptanalysis and Improvement of a Quantum Network System of QSS-QDC Using χ -Type Entangled States**
GAO Gan, FANG Ming, CHENG Mu-Tian
- 110401 **Dynamics of Apparent Horizons in $(N+2)$ -Dimensional Space-Times**
S. S. Zade
- 110701 **High Performance Humidity Sensor Based on Electrospun $\text{Zr}_{0.9}\text{Mg}_{0.1}\text{O}_{2-\delta}$ Nanofibers**
SU Mei-Ying, WANG Jing, YAO Peng-Jun, DU Hai-Ying

THE PHYSICS OF ELEMENTARY PARTICLES AND FIELDS

- 111101 **Triple Z^0 -Boson Production in a Large Extra Dimensions Model at the International Linear Collider**
JIANG Ruo-Cheng, LI Xiao-Zhou, MA Wen-Gan, GUO Lei, ZHANG Ren-You
- 111401 **Re-estimation of the Upper Limit on the Photon Mass with the Solar Wind Method**
LIU Lin-Xia, SHAO Cheng-Gang

NUCLEAR PHYSICS

- 112101 **Fully Self-Consistency in Relativistic Random Phase Approximation**
YANG Ding, CAO Li-Gang, MA Zhong-Yu
- 112501 **Anomalous Neutron Burst Emissions in Deuterium-Loaded Metals: Nuclear Reaction at Normal Temperature**
JIANG Song-Sheng, XU Xiao-Ming, ZHU Li-Qun, GU Shao-Gang, RUAN Xi-Chao, HE Ming, QI Bu-Jia

ATOMIC AND MOLECULAR PHYSICS

- 113201 **Population Evolution of Rydberg Rubidium Atoms by Half-Cycle Pulses**
JIA Guang-Rui, ZHAO Yue-Jin, ZHANG Xian-Zhou, LIU Yu-Fang, YU Kun
- 113202 **Theoretical Analysis of $4f$ and $5p$ Inner-Shell Excitations of W-W^{3+} Ions**
CAO Xiang-Nian, SU Mao-Gen, SUN Dui-Xiong, FU Yan-Biao, DONG Chen-Zhong

FUNDAMENTAL AREAS OF PHENOMENOLOGY(INCLUDING APPLICATIONS)

- 114101 **Extraordinary Transmission through Fractal-Featured Metallic and Superconducting Films at Terahertz Frequency**
LIANG Lan-Ju, JIN Biao-Bing, ZHANG Qiu-Yi, WU Jing-Bo, BAO Yong-Jun, JIA Tao, JIA Xiao-Qing, CAO Chun-Hai, KANG Lin, XU Wei-Wei, CHEN Jian, WU Pei-Heng

- 114102 Compact Ultra-wideband Microstrip Antenna with Metamaterials**
XIONG Han, HONG Jin-Song, ZHU Qing-Yi, JIN Da-Lin
- 114201 A Field Tunable Multichannel Microwave Delay-Line Using a Piezoelectric-Piezomagnetic Superlattice**
TANG Zheng-Hua, ZHANG Wei-Yi
- 114202 A Q-Switched Erbium-Doped Fiber Laser with a Carbon Nanotube Based Saturable Absorber**
S. W. Harun, M. A. Ismail, F. Ahmad, M. F. Ismail, R. M. Nor, N. R. Zulkepely, H. Ahmad
- 114203 Analysis of Responsivity and Signal-to-Noise Ratio in PEPT**
ZHOU Quan, GUO Shu-Xu, LI Zhao-Han, SONG Jing-Yi, CHANG Yu-Chun
- 114204 Performance of Post-Nonlinearity Compensation for Differential-Phase-Shifted-Keying Links with Transmitter Imperfections**
YUAN Jie, XUE Tian-Ming, ZHU Guang-Hao
- 114205 Photon Counting for a Number State Passing through a Laser Channel**
WANG Chang-Chun, YUAN Hong-Chun, FAN Hong-Yi
- 114206 Graphene-Oxide-Based Q-Switched Fiber Laser with Stable Five-Wavelength Operation**
ZHAO Jun-Qing, WANG Yong-Gang, YAN Pei-Guang, RUAN Shuang-Chen, CHENG Jian-Qun, DU Ge-Guo, YU Yong-Qin, ZHANG Ge-Lin, WEI Hui-Feng, LUO Jie, Yuen H. Tsang
- 114207 Large Signal Circuit Model of Two-Section Gain Lever Quantum Dot Laser**
Ashkan Horri, Seyede Zahra Mirmoeini, Rahim Faez
- 114208 An Octave-Spanning, Kerr-Lens Mode-Locked Ti:sapphire Oscillator with Double-Chirped Mirrors and BaF₂**
ZHANG Long, HAN Hai-Nian, ZHANG Qing, WEI Zhi-Yi
- 114209 Decay-Induced Interference Effect on Photon Correlation in a Nearly Equispaced Three-Level Ladder Atom**
CHEN Yao, WANG Fei, SHI Wen-Xing, XIAO Ming
- 114210 Surface Enhanced Raman Scattering Characterization of the ZnO Films Modified with Silver Quantum Dot**
ZHANG Li-Sheng, FANG Yan, WANG Pei-Jie
- 114211 A Practical Approach to Synthesize Multi-channel Fiber Bragg Grating with Right-Angled Triangular Spectrum**
YU Xue-Lian, YAO Yong, XIAO Jun-Jun, TIAN Jia-Jun
- 114212 Beam Manipulation by Metallic Nanoslit Arrays with Perpendicular Cuts inside Slits**
HAO Zhi-Qiang, LI Yu-Dong, CHEN Jing, CHEN Zong-Qiang, XU Jing-Jun, SUN Qian
- 114213 Design and Characterization of a Top Cladding for Silicon-on-Insulator Grating Coupler**
Nemkova Anastasia, XIAO Xi, YANG Biao, CHU Tao, YU Jin-Zhong, YU Yu-De
- 114214 All-or-Nothing-Type Kochen-Specker Experiment with Thermal Lights**
SONG Xin-Bing, WANG Hai-Bo, XIONG Jun, ZHANG Xiang-Dong
- 114215 Novel Optical Parametric Amplifier at 1572 nm Wavelength Using KTP Crystal**
LI Huan-Huan, LI Shi-Guang, MA Xiu-Hua, WANG Jun-Tao, ZHU Xiao-Lei
- 114216 High Current Transfer Ratio Organic Optocoupler Based on Tandem Organic Light-Emitting Diode as the Input Unit**
YANG De-Zhi, SUN Heng-Da, CHEN Jiang-Shan, MA Dong-Ge
- 114217 Theoretical and Experimental Study of a Numerical Aperture for Multimode PCS Fiber Optics Using an Imaging Technique**
Saman Q. Mawlud, Nahlah Q. Muhamad
- 114301 Broadband Acoustic Transmission Enhancement through a Structured Stiff Plate with Locally Resonant Elements**
LI Yong, LIANG Bin, ZOU Xin-Ye, CHENG Jian-Chun
- 114302 Approximation Approach of Realizing an Arbitrarily Shaped Acoustic Cloak with Homogeneous Isotropic Materials**
GAO Dong-Bao, ZENG Xin-Wu

- 114601 Thermo-Mechanical Influence on the Internal Friction of a 51CrV4 Shaft**
J. Göken, I. S. Golovin, T. S. Andrianova, K. Steinhoff, H. Brink
- 114701 Three-Dimensional Parallel Simulation of Formation of Spinning Detonation in a Narrow Square Tube**
HUANG Yue, JI Hua, LIEN Fue-Sang, TANG Hao
- 114702 Observation of Nucleate Boiling on a Fine Copper Wire with Superhydrophobic Micropatterns**
WANG Xin-Wei, SONG Yong-Xin, WANG Hao
- 114703 Non-Newtonian Power-Law Fluid Flow over a Shrinking Sheet**
FANG Tie-Gang, TAO Hua, ZHONG Yong-Fang
- 114704 Mixed Convection Stagnation Point Flow of Casson Fluid with Convective Boundary Conditions**
T. Hayat, S. A. Shehzad, A. Alsaedi, M. S. Alhothuali
- 114705 Analytical and Numerical Approaches to Squeezing Flow and Heat Transfer between Two Parallel Disks with Velocity Slip and Temperature Jump**
Amjad Hussain, Syed Tauseef Mohyud-Din, Taqi Ahmed Cheema

PHYSICS OF GASES, PLASMAS, AND ELECTRIC DISCHARGES

- 115201 Solution of Magnetohydrodynamic Oscillations in Electrolytes with Ion-Neutral Collisions**
LIU Yuan-Tao, ZHAO Hua, LI Lei, FENG Yong-Yong

CONDENSED MATTER: STRUCTURE, MECHANICAL AND THERMAL PROPERTIES

- 116201 An Effective Solution for the Best Set of Beveling Parameters of the Cubic High-Pressure Tungsten Carbide Anvil**
HAN Qi-Gang, ZHANG Qiang, LI Ming-Zhe, JIA Xiao-Peng, LI Yue-Fen, MA Hong-An
- 116801 Thermoelastic Stress in a Functionally Graded Infinite Plate with Electromagnetic Wave Absorption**
TIAN Hong-Yan, WANG Xing-Zhe, ZHOU You-He

CONDENSED MATTER: ELECTRONIC STRUCTURE, ELECTRICAL, MAGNETIC, AND OPTICAL PROPERTIES

- 117101 Tunable UV Absorption and Mobility of Yttrium-Doped ZnO using First-Principles Calculations**
BAI Li-Na, SUN Hai-Ming, LIAN Jian-She, JIANG Qing
- 117102 First-Principles Study of Electronic Structure and Optical Properties of Cubic Perovskite CsCaF₃**
K. Ephraim Babu, A. Veeraiah, D. Tirupati Swamy, V. Veeraiah
- 117103 Growth and Characterization of an a-Plane In_xGa_{1-x}N on a r-Plane Sapphire**
ZHAO Gui-Juan, LI Zhi-Wei, WEI Hong-Yuan, LIU Gui-Peng, LIU Xiang-Lin, YANG Shao-Yan, ZHU Qin-Sheng, WANG Zhan-Guo
- 117104 A Hybrid Density Functional Theory Study of Band Gap Tuning in ZnO through Pressure**
ZHAO Bo-Tao, DUAN Yi-Feng, SHI Hong-Liang, QIN Li-Xia, SHI Li-Wei, TANG Gang
- 117201 Photo-Induced Electron Spin Polarization in a Narrow Band Gap Semiconductor Nanostructure**
A. John Peter, Chang Woo Lee
- 117302 The Formation of Exciplex and Improved Turn-on Voltage in a Hybrid Organic-Inorganic Light-Emitting Diode**
ZHANG Yan-Fei, ZHAO Su-Ling, XU Zheng, KONG Chao
- 117303 Transport through a Gate Tunable Graphene Double Quantum Dot**
ZHOU Cheng, TU Tao, WANG Li, LI Hai-Ou, CAO Gang, GUO Guang-Can, GUO Guo-Ping
- 117901 Formula for the Probability of Secondary Electrons Passing over the Surface Barrier into a Vacuum**
XIE Ai-Gen, XIAO Shao-Rong, ZHAN Yu, ZHAO Hao-Feng

CROSS-DISCIPLINARY PHYSICS AND RELATED AREAS OF SCIENCE AND TECHNOLOGY

- 118101 Structural and Optical Behavior of Germanium Quantum Dots**
ALIREZA Samavati, Z. Othaman, S. K. Ghoshal, M. R. Dousti, R. J. Amjad
- 118102 Preparation and Characterization of Fe-Based Metallic Glasses with Pure and Raw Elements**
Nassima Seghairi, Badis Bendjemil, Gabriel Lavorato, Alberto Castellero, Marcello Baricco
- 118103 Orientation and Structure of Controllable GaAs Nanowires Grown on GaAs (311)B Substrates by Molecular Beam Epitaxy**
ZHAO Zhi-Fei, LI Xin-Hua, WEN Long, GUO Hao-Min, BU Shao-Jiang, WANG Yu-Qi
- 118501 High Sensitivity Magnetic Field Sensors Based on Nano-Polysilicon Thin-Film Transistors**
ZHAO Xiao-Feng, WEN Dian-Zhong, ZHUANG Cui-Cui, LIU Gang, WANG Zhi-Qiang
- 118502 Structural Design of a Compact in-Plane Nano-Grating Accelerometer**
YAO Bao-Yin, ZHOU Zhen, FENG Li-Shuang, WANG Wen-Pu, WANG Xiao
- 118503 Ultra Low Dark Current, High Responsivity and Thin Multiplication Region in InGaAs/InP Avalanche Photodiodes**
LI Bin, YANG Huai-Wei, GUI Qiang, YANG Xiao-Hong, WANG Jie, WANG Xiu-Ping, LIU Shao-Qing, HAN Qin
- 118701 Preliminary Study on Neutron Radiography with Several Hundred keV Fast Neutrons**
LI Hang, ZOU Yu-Bin, LU Yuan-Rong, GUO Zhi-Yu, TANG Guo-You
- 118901 Promotion of Cooperation in a Spatial Public Goods Game with Long Range Learning and Mobility**
XIAO Yao, HUA Da-Yin

JUST FOR AUTHORS
— CHINESE PHYSICS LETTERS